P4B.8

Freezing Level Determinations with Polarimetric Radar: Retrieval Model and Application

Kyoko Ikeda* and Edward A. Brandes
National Center for Atmospheric Research, Boulder, Colorado

1. Introduction

Backscattered signals from dual-polarization radars provide information regarding hydrometeor size, shape, orientation, and thermodynamic phase in precipitating storms. Because polarimetric measurements are particularly sensitive to the presence of large, wetted particles that characterize melting layers, response signatures in the measurements can be used to designate freezing levels. Previous studies to determine freezing levels have focused on reflectivity measurements (White et al. 2002; Mittermaier and Illingworth 2003). In this study we present a freezing level detection algorithm that exploits melting layer signatures in vertical profiles of radar reflectivity (Z_H), linear depolarization ratio (LDR), and co-polar correlation coefficient (ρ_{HV}). Response signals from LDR and ρ_{HV} during hydrometeor phase changes are more pronounced than that for reflectivity, often allowing determination of the freezing level when signatures in Z_H are absent. Moreover, consensus estimates from the three parameters should reduce errors in the estimates compared with those derived solely from Z_H.

The algorithm has been applied to radar data collected from a number of field campaigns. Performance is demonstrated with a multiple freezing level event observed in the Oregon Cascades during the Improvement of Microphysical PaRametrization through Observational Experiments (IMPROVE) II field campaign. Although melting and freezing occur at the wet-bulb 0^{o}C level, the current algorithm is designed to retrieve dry-bulb zeroes. For saturated environments, as expected with upslope conditions in the Cascades, both temperatures occur at the same height. For unsaturated conditions, wet-bulb zeroes occur at a lower level. Examination of high resolution aircraft data from several events occurring during other field programs revealed that wet-bulb zero depressions were 0-105 m. The accuracy in freezing level heights deduced with the proposed algorithm is believed to be 100-200 m.

2. Overview of the freezing level detection algorithm

Typical vertical radar profiles through the melting layer disclose radar reflectivity (Z_H), linear depolarization ratio (LDR), and differential reflectivity (Z_{DR}) maxima and a co-polar correlation coefficient (ρ_{HV}) minimum just below the 0^{o}C level (Fig. 1). The onset of melting changes the density and dielectric factor of frozen hydrometeors (Fabry and Zawadzki 1995) causing them to behave as raindrops of equivalent size and increasing their reflectivity (Battan 1973; Chapter 10). Further increase in Z_H results as wetted hydrometeors become sticky and aggregation occurs. Eventually, melting hydrometeors collapse into raindrops and an increase in terminal velocity removes them from the sample volume. The net effect is a rapid decrease in reflectivity.

Melting snowflakes and aggregates wobble as they fall creating a distribution of canting angles. Particle canting causes a small portion of the transmitted energy to "leak" into the orthogonal direction. The leakage is enhanced for large mixed-phased particles and creates a distinct LDR maximum in the melting layer. Correlations between horizontally and vertically polarized signals are typically close to unity for pristine ice crystals and raindrops. However, changes in hydrometeor shapes and the presence of mixed-phased precipitation cause ρ_{HV} to decrease to <0.93 in the melting layer. Snow aggregates do not have preferred orientations; therefore they have small Z_{DR} (<0.5 dB). Raindrops are flattened and tend to orient themselves with their major axes near horizontal, causing Z_{DR} to be 0.3–4 dB. Often Z_{DR} has a maximum value in the melting layer indicating large aspect ratios associated with partly-melted hydrometeors.

The principal idea behind the freezing level detection algorithm lies in identifying the heights at which the melting layer signature extremes discussed above exist and using statistical relationships between the signatures and the 0^{o}C level. Fig. 2 shows the depression of melting layer signature extremes for LDR, ρ_{HV}, and Z_{DR} from the height of the reflectivity bright band maximum. The data are from over 300 radar profiles obtained from constant antenna elevation scans collected on 5 September 1998 during the PRECIP98 field campaign. Vertical distributions of each parameter were calculated by averaging measurements over 10-degree sectors at elevation angles between 4 and 12 degrees. Examination reveals that LDR and ρ_{HV} extremes typically occur 200 m below the Z_H maximum while the maximum Z_{DR} occurs 200-300 m below the Z_H maximum. The depression distributions are narrow for LDR and ρ_{HV}, and their extremes generally occur at the same heights. The depression distributions for Z_{DR}, on the other hand, are broad and often 500 m or more below that for reflectivity. Also, there is no melting layer signature for Z_{DR} at vertical incidence or in many convective situations. Consequently, only Z_H, LDR, and ρ_{HV} are used for designating the 0^{o}C level in the proposed algorithm.

* *Corresponding author address:* Kyoko Ikeda, National Center for Atmospheric Research, P.O. Box 3000, Boulder, CO 80307
E-mail: kyoko@ncar.ucar.edu

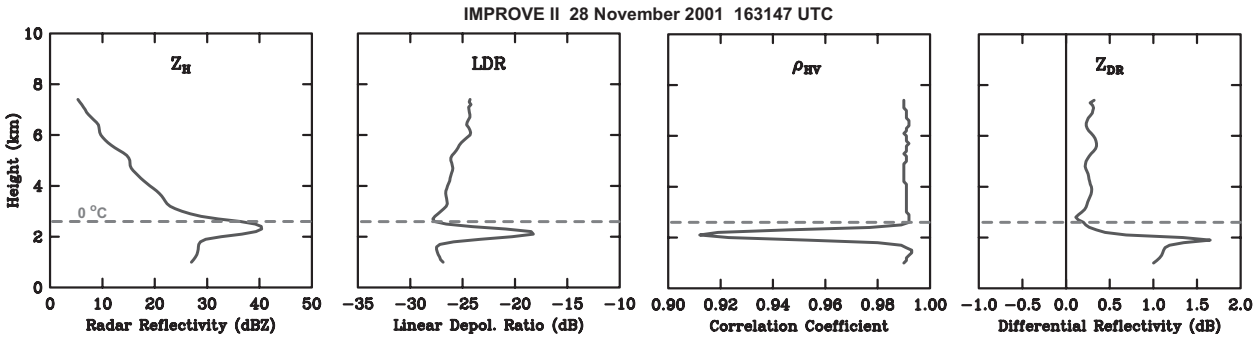

Figure 1: Profiles of radar reflectivity (dBZ), linear depolarization (dB), correlation coefficient, and differential reflectivity (dB) from 28 November 2001 163147 UTC. The 0°C level at 2.53 km is an average of two soundings.

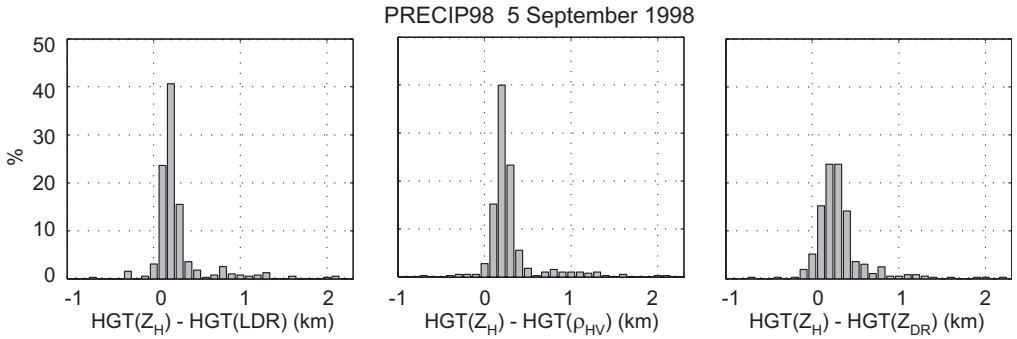

Figure 2: Frequency distributions showing the offsets of the LDR, ρ_{HV}, and Z_{DR} extremes [HGT(LDR), HGT(ρ_{HV}), and HGT(Z_{DR})] from the Z_H maxima [HGT(Z_H)].

A composite of LDR and ρ_{HV} depressions from PRECIP98 (Florida), STEPS (eastern Colorado), CASES (Kansas), TRMM-LBM (Brazil), MAP (Italy), and IMPROVE (northwestern U.S.) field projects suggests that offsets of the LDR and ρ_{HV} extremes from the Z_H maximum are typically 200 m for warm season datasets, whereas an offset of 100 m is likely for cold season datasets (MAP and IMPROVE). However, examination of individual profiles reveals that larger offsets associate with more intense precipitation.

Fig. 3 shows model profiles developed from the observed relations of melting layer signatures discussed above. Freezing level designations begin by identifying the melting layer extremes in the observed vertical profiles. Extremes in the observed and modeled profiles are aligned, and the correlation coefficient between the observed and modeled profile is calculated to determine the degree of fit. When the observed distribution roughly matches the melting layer signature in the model, the correlation is high. Melting layer signatures are accepted by the algorithm when correlation coefficients are greater than 0.7. This threshold value was chosen because one half of the variability in the observations is explained by the model at this value. Freezing level determination is then made by knowing the statistical offset between the typical 0°C level and the heights of the Z_H, LDR, and ρ_{HV} extremes. The offset was 300 m for Z_H and 500 m for LDR and ρ_{HV} for the PRECIP98 dataset. The offsets of

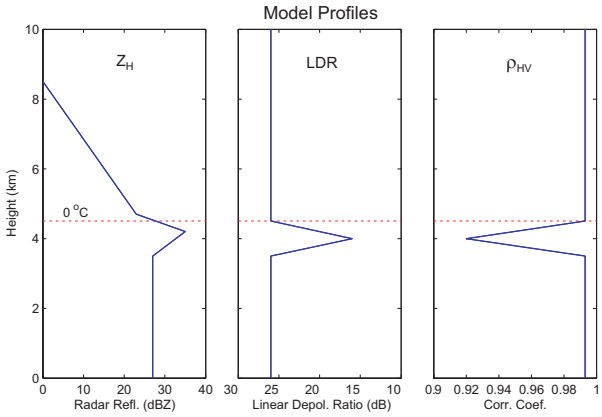

Figure 3: Sample model vertical profiles of radar reflectivity, linear depolarization ratio, and correlation coefficient.

200 m for Z_H and 300 m for LDR and ρ_{HV} were used for the IMPROVE dataset. Then the estimated freezing level height for the *i*th parameter (with 1 for Z_H, 2 for LDR, and 3 for ρ_{HV}) is

$$h_i = ht_i + offset_i \qquad (1)$$

for the height of the melting layer signature extreme ht_i. Resulting estimates from the three parameters typically vary. A consensus (weighted) estimate is then computed from

$$h_{fzlv} = \sum_{i=1}^{n} h_i r_i^2 \Big/ \sum_{i=1}^{n} r_i^2 \qquad (2)$$

where n is the number of parameters with a correlation coefficient (r) above the threshold value, and h_i and r_i are the freezing level height and correlation coefficient for the ith parameter, respectively. When only one profile meets the threshold criteria, the consensus freezing level height is not calculated. The measure of scatter among the estimates is expressed with the standard deviation σ,

$$\sigma = \sqrt{\frac{1}{n}\sum_{i=1}^{n}(h_i - h_{fzlv})^2} \qquad (3)$$

This value serves as confidence factor for the retrieval.

3. Application of the freezing level algorithm

In this section algorithm performance is demonstrated with a dataset collected over the Oregon Cascades during the IMPROVE II field campaign. On 28 November 2001 a large synoptic low pressure system approached the Cascades region from the northeastern Pacific Ocean. By 1200 UTC, the low pressure center was located to the west of Vancouver Island, British Columbia and the associated warm and cold fronts were advancing across the northwestern coastal U.S.

Radar data indicated that warm frontal precipitation over the IMPROVE domain was most intense between 0930 and 1000 UTC. Soon afterward the radar displayed multiple freezing levels for 20-40 minutes. Fig. 4 is a vertical cross-section from 1009 UTC for an azimuth of 250°. In the figure the lower melting layer is located ~0.7 km above ground level (AGL). The elevated melting layer is at ~2.3 km AGL. The figure also shows a sloped band of high reflectivity between 1.5 km AGL and the surface at a range of 11-17 km. [The slope is different from that expected for a rain streak because the horizontal wind was generally from the southwest (toward the right in the figure). Consequently, the sloping band is also believed to be connected with melting hydrometeors.]

Fig. 5 is a time series of Z_H and LDR profiles between 0906 and 1121 UTC. Consensus freezing levels deduced from the algorithm are superimposed. ρ_{HV} profiles are not shown because the identified melting layers were essentially the same as those from LDR measurements. The profiles were constructed from range-height-indicator scans (RHI) by averaging measurements 3 km in the horizontal and 0.2 km in the vertical at a distance of 8 km for the same azimuth as in Fig. 4. Multiple freezing levels were detectable for all quadrants in which RHI scans were performed, but measurements from the azimuth of 250° were least contaminated by ground clutter from nearby mountains. Fig. 5 suggests that the lower freezing level rose from 1.05 km at 0906 UTC to 1.3 km MSL at 1009 UTC. Afterward, it descended slightly, dissipating by 1029 UTC.

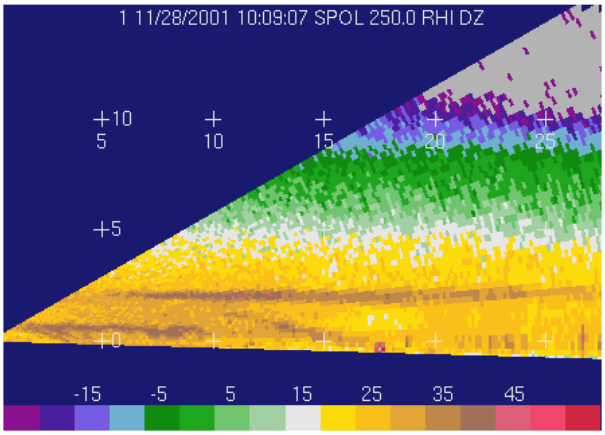

Figure 4: Vertical cross-section of radar reflectivity at an azimuth of 250°. The ordinate is height above ground level. The radar site is at an elevation of 0.457 km.

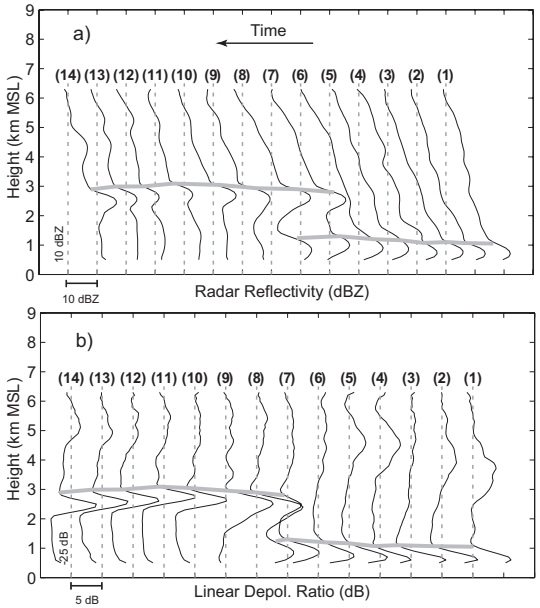

(1) 0906 UTC (4) 0937 UTC (7) 1009 UTC (10) 1040 UTC (13) 1110 UTC
(2) 0917 UTC (5) 0948 UTC (8) 1019 UTC (11) 1050 UTC (14) 1121 UTC
(3) 0927 UTC (6) 0958 UTC (9) 1029 UTC (12) 1100 UTC

Figure 5: Vertical profiles of a) radar reflectivity (dBZ) and b) linear depolarization ratio (dB) from 0906 to 1121 UTC at an azimuth of 250° and a range of 8 km. Gray bold lines are consensus freezing level heights from Z_H, LDR and ρ_{HV}. Dashed vertical lines represent a)10 dBZ and b) –25 dB with respect to each profiles. Tick mark increments are equivalent to a) 10 dBZ and b) 5 dB.

An elevated freezing level first appeared in the Z_H and LDR profiles at 1009 UTC and a height of 2.73 km MSL. The Z_H signature for the elevated freezing level was the strongest at this time and weakened as precipitation decreased. The LDR signature intensified to –17.3 dB by 1029 UTC. According to the consensus estimates, the elevated freezing level rose initially to 3.09 km at 1050 UTC and descended to 2.89 km MSL by 1121 UTC.

Synoptic analyses indicate that evolution of the two freezing levels responded to motion of the low pressure center and its associated warm front. While the surface warm front was well upstream of the radar, a single freezing level was low to the ground. As the warm air advanced, the elevated freezing level appeared. The lower freezing level eventually dissipated as the surface warm front passed the profile location, and only the elevated freezing level remained. A frontal temperature inversion near the 0^oC level was observed with a sounding released at 1100 UTC from Salem, Oregon (60 km northwest of the radar site). The sounding found the upper and lower freezing levels to be 2.70 and 1.03 km MSL, respectively, in agreement with the estimated freezing level heights.

Over the next six hours the elevated freezing level fell an additional 0.3 km. With cold frontal passage between 1700-1800 UTC, the freezing level rapidly descended to 1.7 km MSL by 2200 UTC (Fig. 6). Data points in Fig. 6 are estimates of freezing level heights over a gridded domain (35x35 km) in the eastern sector of the radar. The 0^oC levels from observations are also plotted. Generally, freezing level heights from Z_H have larger variability than those from other parameters. Scatter in the designations are more pronounced after 1730 UTC for all parameters. This is due to broadening freezing level height distributions over the domain from weakening precipitation and descending freezing level caused by passage of the surface cold front.

4. Summary and concluding remarks

A freezing level detection algorithm that utilizes polarimetric measurements has been described. The algorithm looks for melting layer signatures in the radar parameters and applies a statistical offset between the 0^oC level and the signature heights. Determinations are typically good when radar signals are strong. Moreover, sensitivity of LDR and ρ_{HV} to mixed-phased hydrometeors often make designations possible when signatures are absent in Z_H measurements. The error with the algorithm is on the order of 100 to 200 m. Algorithm enhancement is possible by taking into account the precipitation intensity dependencies of the 0^oC-depressions. The algorithm readily makes retrievals for distances to ~50 km. At greater distances radar beam broadening make precise determinations difficult.

The algorithm was applied to a dataset collected over the northwestern U.S. on 28 November 2001. Evolution of the two observed freezing levels responded to the movement of the synoptic low pressure center and its associated fronts. Initially, a single freezing level existed near ground. An advancing warm front warmed the lower atmosphere and created the elevated freezing level. Passage of the surface front and continued warming eventually overwhelmed the lower melting layer. Later, cold front passage caused a rapid lowering of the elevated freezing layer.

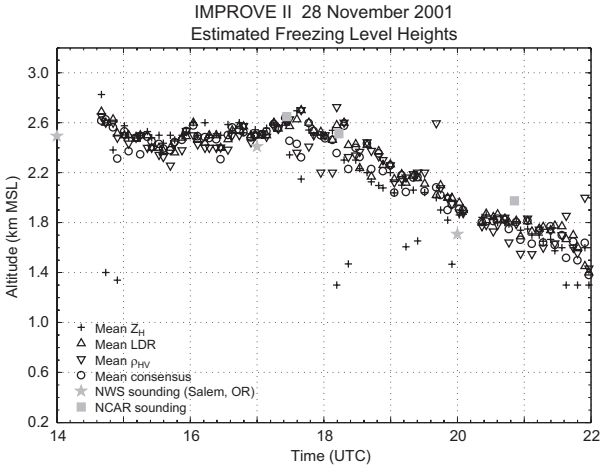

Figure 6: Time series of freezing level estimates for 1400-2200 UTC on 28 November 2001. The estimates from Z_H, LDR, and ρ_{HV} were obtained over a gridded domain in the eastern sector of the radar. "Mean" of each parameter is the weighted mean over the domain, computed using the correlation coefficient between the model and observed vertical profile. "Mean consensus" values were obtained similarly, except the reciprocal of σ from Equation 3 was used for weighting. The NCAR sounding location on this day was ~52 km southwest of the radar site, at an elevation of 0.24 km.

Acknowledgement: This work was supported by the Federal Aviation Weather Research Program and is in response to requirements of the FAA. The views expressed are those of the authors and do not necessarily represent the official policy of the U.S. government.

References

Battan, L. J., 1973: *Radar Observation of the Atmosphere*, University of Chicago Press, 324pp.

Fabry, F., and I. Zawadzki, 1995: Long-term radar observations of the melting layer of precipitation and their interpretation. *J. Atmos. Sci.,* **52,** 838-851.

Mittermaier, M. P., and A. J. Illingworth, 2003: Comparison of model-derived and radar-observed freezing-level heights: Implications for vertical reflectivity profile-correction schemes. *Quart. J. Roy. Meteor. Soc.,* **129,** 83-95.

White, A. B., D. J. Gottas, E. T. Strem, F. M. Ralph, and P. J. Neiman, 2002: An automated brightband height detection algorithm for use with Doppler radar spectral moments. *J. Atmos. Oceanic. Technol.,* **19,** 687-697.